

# Synthesis, Crystal Structure and Bonding Analysis of Intermetallic Compound $\text{BaAu}_3\text{Zn}_2$

Trinath Mishra <sup>a</sup>, Ram Dulare <sup>a\*</sup>

<sup>a</sup> Department of Chemistry, Post Graduate College, Ghazipur, 233001 U. P., India

\*Corresponding author, E-mail address: [rdxpgcchem@gmail.com](mailto:rdxpgcchem@gmail.com)

## ABSTRACT

The intermetallic compound  $\text{BaAu}_3\text{Zn}_2$  has been synthesized through fusion of stoichiometric metals in sealed Ta tube at 800 °C using high-frequency furnace followed by annealing at 400°C for two weeks. The synthesized compound characterized by powder, single crystal X-ray diffraction techniques.  $\text{BaAu}_3\text{Zn}_2$  crystallized in the orthorhombic system with space group  $Pnma$  and Pearson symbol -  $oP24$  and utilizes the same set of Wyckoff sequence ( $dc^4$ ) as  $\text{SrZn}_5$  structure where Au atoms replace Zn atoms on  $4c$  Wyckoff sites with different bonding patterns. The structure contains three structural motifs (a) Hexagonal-diamond-like gold host lattice (b) Interstitial Ba atoms (blue) and (c) Infinite linear chains along  $b$  axis formed by only Zn atoms (green). Bonding analyses indicate a typical polar intermetallic behavior for  $\text{BaAu}_3\text{Zn}_2$ .

**Keywords:** Polar intermetallics; gold rich phases; LMTO-ASA approximation; isotropic deformation; DOS and COHP calculations; X-ray diffraction.

## 1. Introduction

Intermetallic compounds represent an extensive pool for energy related applications originated from magnetic, electric, optic, caloric and catalytic properties. The discovery of novel intermetallic compounds can extend understanding of the principles that govern structural stability and chemical bonding as well as to find new applications. Electron-poor polar intermetallics have fairly attracted the attention in field of solid-state chemistry [1]. Several studies show that the formation of certain structure is very challenging task to understand even similarity in their composition or valence electron counts.

It has been reported that gold does not behave as a noble metal in intermetallics [2,3]. Au rich intermetallics are a fertile field to discover new valence electron-poor polar intermetallics. The structural diversity of gold in intermetallic compounds is wider than that of other noble metals. The key parameter explaining the peculiar crystal chemical behavior relies in relativistic effects, bonding of gold leading to enhanced  $6s$ - $5d$  mixing in valence state as well as smaller effective radius and an enhanced electronegativity, closest to the values of Se and Te and hence the shorter bonds [4]. The survey of the binary alkaline earth and rare earth gold phases reveals quite different gold substructures with a direct dependence on the gold content. Therefore, gold exhibits stronger bonding interactions with itself and other anionic elements below the  $E_F$  due to significant covalent bonding interactions with gold and other electronegative components [5]. Valence electron-poor polar intermetallic with valence electron counts ( $VEC$ ) between 2.0 and 3.0  $e^-$ /atom show a plethora of unique and interesting structural motifs and bonding features. Therefore, establishing simple structure bonding property relationships is especially challenging for this class of compound because commonly accepted valence electron counting rules are inappropriate.

The gold rich phases *i.e.*,  $\text{Ba}_2\text{Au}_6(\text{Au},\text{T})_3$  ( $\text{T} = \text{Zn}, \text{Cd}, \text{Ga}, \text{In}, \text{Sn}$ ) exhibit never done hexagonal-diamond-like gold host lattice, where the channels extending along the  $c$  axis are filled by ordered large cations and  $(\text{Au},\text{T})_3$  triangles [5]. The identical motifs are observed in  $\text{Sr}_2\text{Au}_6(\text{Au}_{3-x}\text{T}_x)$  ( $\text{T} = \text{Zn}, \text{Ga}$ ) for  $x = 2.5$ - $2.9$ , with a distortion in monoclinic symmetry appear for  $x = 2.2$ - $2.3$  [6]. The slight changes in size and  $VEC$  could lead to a phase transition *via* structural relaxation [7, 8]. Similarly, matrix effect is quite observed in  $\text{CaZn}_2\text{Au}_4$  [9]. Few quasicrystals and their corresponding approximants with  $e/a$  values (ca. 1.7-2.2) have also been reported as a different type of Hum-Rothery Phases [10].

In light of aforementioned findings and in continuation of the our phase analytical studies we have now obtained a new and novel compound  $BaAu_3Zn_2$ . Herein we report the synthesis and structural characterization of the  $BaAu_3Zn_2$  phase and discussed their topological relationship with the simple binary  $SrZn_5$  structure. Theoretical analyses have also been provided which helps to understand the highly delocalized bonding states among the component atoms with their characteristically high coordination numbers.

## 2. Experimental

### 2.1. Syntheses

Starting materials were Ba pieces (99.95 %, Alfa Aesar), as received Au particles (99.999 %, BASF) and Zn shot (99.99%, Alfa Aesar). Prior to the reactions, the Ba was washed with dried cyclohexane and kept in Schlenk tubes under purified argon. All reactants and products were handled in a glovebox filled with dry  $Ar_2$  ( $\leq 0.1$  ppm  $H_2O$  per volume).

The desired compound was synthesized *via* high-temperature reactions. The weighed reactants were weld-sealed into pre-cleaned Ta containers that was subsequently enclosed in evacuated silica jackets ( $< 10^{-5}$  Torr) to protect the Ta from air oxidation.

The crystals of  $BaAu_3Zn_2$  were first obtained as a minor product (~40%) which on reaction with a nominal composition of  $Ba_2Au_6Zn_3$  heated at 800 °C for 10 h, cooled at 400 °C, annealed there for two weeks and finally quenched in water. After the desired chemical composition establishment by a single crystal structural refinement, stoichiometric reactions with  $BaAu_{3+x}Zn_{2-x}$  ( $x = 0, \pm 0.2$ ) compositions were run similarly to the check the phase width. Highest yield (>85 vol %) was obtained for ( $x = 0$ ) *i.e.* loaded  $BaAu_3Zn_2$  composition whereas ( $x = \pm 0.2$ ) compositions yielded the major  $BaAu_3Zn_2$  phase along with other unknown impurities.

The polycrystalline  $BaAu_3Zn_2$  sample have metallic lusters and air stable for two months at RT. The single crystals suitable for X-ray analyses were easily separated out from crushed sample and remaining powder were for phase analyses.

### 2.2. X-ray Diffraction Studies

The polycrystalline sample of  $BaAu_3Zn_2$  was ground to fine powders under dry paraffin oil and studied the X-ray powder diffraction using the STADI P powder diffractometer equipped with an area detector limit of ~5 vol % in equivalent scattering power and  $CuK\alpha$  radiation ( $\lambda = 1.54059 \text{ \AA}$ ). The phase identification was done using PowderCell program [11] and lattice parameters were refined with the aid of the UnitCell program [12]. The comparison of loaded sample and calculated patterns obtained using Jana2006 [13] is given in Figure 1.

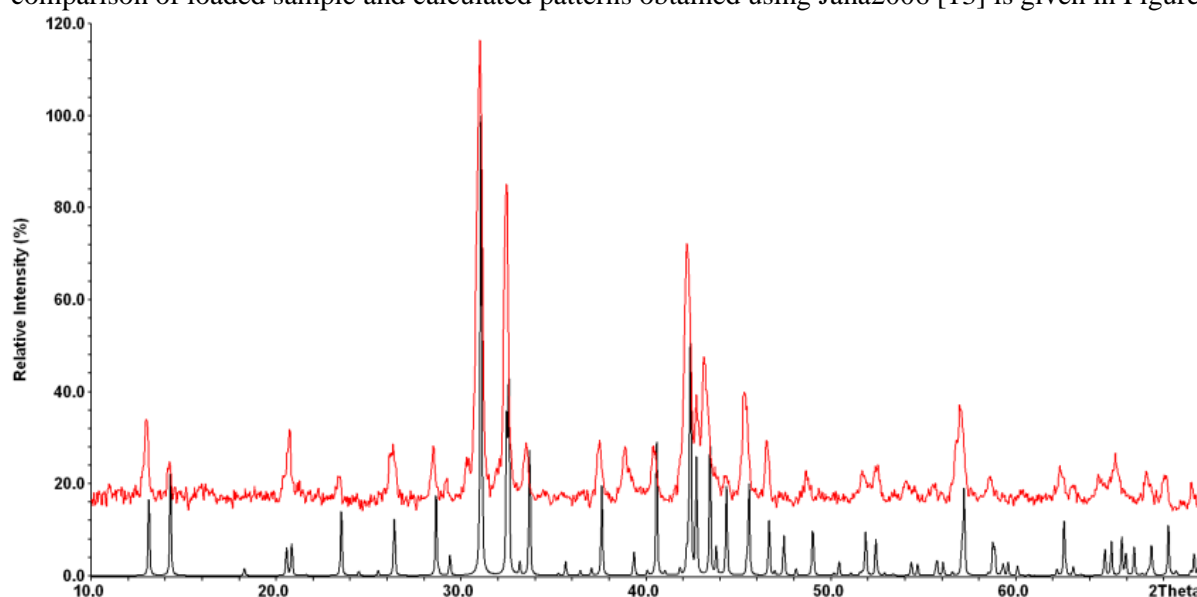


**Figure 1.** Powder pattern of loaded product (top, red) and calculated patterns derived from single crystal data (bottom, black) for  $BaAu_3Zn_2$ .

Single crystals of BaAu<sub>3</sub>Zn<sub>2</sub> were selected carefully from the samples, sealed in capillary in a Ar<sub>2</sub>-filled glovebox and then mounted on a Bruker SMART APEX CCD diffractometer equipped with Mo K<sub>α</sub> ( $\lambda = 0.71069 \text{ \AA}$ ) radiation source. Single crystal diffraction data were collected at room temperature in an  $\omega$  scan mode with exposure time of 10 s over the  $2\theta$  range from  $\sim 3^\circ$  to  $\sim 57^\circ$ . The reflection intensities were integrated with the SAINT program in the SMART software package over the entire reciprocal sphere. Empirical absorption corrections were deduced from the SADABS program. The space groups were determined by XPREP and SHELXTL 6.1 [14]. The structure was solved using direct methods and refined on  $|F^2|$ . Details of the crystallographic data for BaAu<sub>3</sub>Zn<sub>2</sub> are listed in Table 1 and atomic coordinates and equivalent isotropic displacement parameters in Table 2.

**Table 1.** Crystal and structural refinement data for BaAu<sub>3</sub>Zn<sub>2</sub>.

Formula weight, g mol <sup>-1</sup>	858.98
Space group, <i>Z</i>	<i>Pnma</i> , 4
Lattice parameters, $\text{\AA}$	$a = 13.490(3)$ $b = 5.493(1)$ $c = 6.976(1)$
Cell volume, $\text{\AA}^3$	$V = 516.9(2)$
Calc. density, g cm <sup>-3</sup>	11.037
Absorption coeff., mm <sup>-1</sup>	101.266
$\square$ range, deg.	3 - 28
Refl. coll. / $R_{\text{int}}$	3662 / 0.0732
Data / restr. / para.	699 / 0 / 35
Goodness-of-fit	0.988
$R1, wR2$ for $I \geq 2\sigma(I)$	0.0361 / 0.0737
$R1, wR2$ for all data	0.0528 / 0.0789
Extinction coefficient	0.00054(9)
Diff. peak / hole, e/ $\text{\AA}^{-3}$	4.103 / -3.469

**Table 2.** Atomic coordinates ( $\times 10^4$ ) and equivalent isotropic displacement parameters ( $\text{\AA}^2 \times 10^4$ ) for BaAu<sub>3</sub>Zn<sub>2</sub>.

Atom	Wyck.	Symm.	<i>x</i>	<i>y</i>	<i>z</i>	$U_{\text{eq}}$
Ba	4 <i>c</i>	. <i>m</i> .	4101(1)	1/4	8577(2)	131(3)
Au1	4 <i>c</i>	. <i>m</i> .	2164(1)	1/4	1652(1)	106(3)
Au2	4 <i>c</i>	. <i>m</i> .	2030(1)	1/4	5638(1)	121(3)
Au3	4 <i>c</i>	. <i>m</i> .	145(1)	1/4	915(1)	129(3)
Zn	8 <i>d</i>	1	3527(1)	0.0009(3)	3631(3)	88(4)

### 2.3. Electronic Structure Calculations

Actually, this method is particularly effective in the case of isotropic deformation modes in order to get composition, structure, bonding properties. Electronic structure calculations for BaAu<sub>3</sub>Zn<sub>2</sub> were performed on the basis of the linear muffin tin orbital atomic sphere approximation (LMTO-ASA) method [15,16]. The radii of the Wigner-Seitz spheres were assigned automatically such that the overlapping potentials would be the best possible approximations to the full potential. No additional empty spheres were added subject to a 16% overlap restriction between atom-centered spheres. All spheres have shown significant and rational radii for Ba, Au(1), Au(2), Au(3) and Zn are 2.30, 1.65, 1.60, 1.58 and 1.45  $\text{\AA}$ , respectively.

The calculation for  $\text{BaAu}_3\text{Zn}_2$  were performed with nonadjacent halves of the split cation sites fully occupied. Basis sets for Ba  $5d$ ,  $6s$ , ( $6p$ ); Au  $5d$ , ( $5f$ ),  $6s$ ,  $6p$  and Zn  $3d$ ,  $4s$ ,  $4p$  (down folded orbitals in parentheses) were employed in the calculations. The band structure was sampled at  $16 \times 16 \times 16$   $k$  points in the irreducible wedge of the Brillouin zone. Crystal orbital Hamilton population (COHP) analyses [17] were also undertaken to get more idea of bonding properties along with charge density calculation to elaborate delocalization effects.

### 3. Results and discussion

#### 3.1. Crystal structure description

According to the lattice parameters, space groups, structural features and single crystal X-ray diffraction analyses  $\text{BaAu}_3\text{Zn}_2$  crystallized in the orthorhombic system with space group  $Pnma$  and Pearson symbol -  $oP24$  (Tables 1 and 2).  $\text{BaAu}_3\text{Zn}_2$  utilizes the same set of Wyckoff sequence ( $dc^4$ ) as  $\text{SrZn}_5$  structure where Au atoms replace Zn atoms on  $4c$  Wyckoff sites, Ba replaces Sr atom on  $4c$  Wyckoff site and one Zn atom retains  $8d$  site. Although  $\text{BaAu}_3\text{Zn}_2$  and  $\text{SrZn}_5$  have similar Pearson symbol -  $oP24$  and same set of Wyckoff sequence ( $dc^4$ ) but they exhibit different bonding patterns, which render them as different structural types [18].  $\text{BaAu}_3\text{Zn}_2$  structure contains the hexagonal-diamond-like gold host lattice which is comparable to the unprecedented hexagonal-diamond-like gold host lattice, observed in the series  $\text{A}_2\text{Au}_6(\text{Au},\text{T})_3$ , ( $\text{A} = \text{Ba}, \text{Sr}$  and  $\text{T} = \text{Al}, \text{Cd}, \text{Ga}, \text{In}, \text{Sn}, \text{Zn}$ ) [19-21].

The present structure contains three structural motifs (a) Hexagonal-diamond-like gold host lattice (b) Interstitial Ba atoms (blue) and (c) Infinite linear chains along  $b$  axis formed by only Zn atoms (green). Interstitial Ba atoms and infinite linear Zn chains are tightly bound within cavities of the hexagonal-diamond-like gold host lattice that is generated by interconnection of  $\text{Au}_6$  hexagonal rings to each other in 3D. Hexagonal rings are formed by Au(1), Au(2) and Au(3) atoms (gold atoms occupy  $4c$  Wyckoff site). The  $8d$  site results in the infinite linear chains of Zn atoms running along  $b$  axis (Figure 2). The Au-Au distances (2.77-3.05 Å) in the present hexagonal-diamond-lattice is shorter than those of hexagonal-diamond-lattice of gold in  $\text{Ba}_2\text{Au}_6(\text{Au},\text{Zn})_3$  (2.91-3.14 Å) which exhibits delocalized bonding patterns. It indicates that the strong Au-Au bonding interactions within the present hexagonal-diamond-lattice of  $\text{BaAu}_3\text{Zn}_2$  structure are expected to be more localized. The Zn-Zn distance (2.74-2.76 Å) is close to the sum of Pauling's metallic radii (2.678 Å), suggesting strong M-M bonding in this chain. The Au-Zn distances vary in a range 2.60-2.81 Å, which is slightly shorter than the average Au-Zn distance of  $\text{Ba}_2\text{Au}_6(\text{Au},\text{Zn})_3$  ( $4 \times 2.68$  Å and  $2 \times 2.86$  Å), reflecting strong interactions between hexagonal-diamond-lattice of gold atoms and linear chain formed by Zn atoms. The environment of interstitial Ba atom formed by Au and Zn atoms results in a cage-like structure (baby carry basket) where central Ba atom is surrounded by ten Au atoms and eight Zn atoms (Figure 3).

The valence electrons per atom (e/a) value for  $\text{BaAu}_3\text{Zn}_2$  is 1.5 with the consideration of Au  $5d^{10}$  states as core which falls within the range of 1.3-1.7 as observed for the series  $\text{A}_2\text{Au}_6(\text{Au},\text{T})_3$ , ( $\text{A} = \text{Ba}, \text{Sr}$  and  $\text{T} = \text{Al}, \text{Cd}, \text{Ga}, \text{In}, \text{Sn}, \text{Zn}$ ) [22, 23].

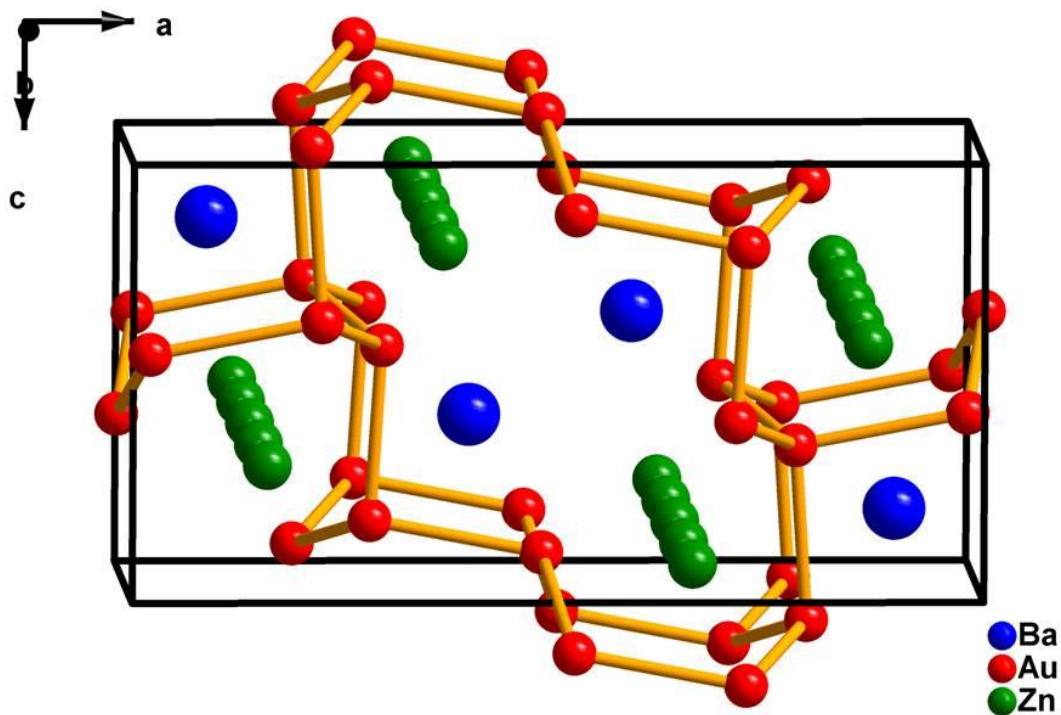


**Figure 2.** Hexagonal-diamond-like gold lattice stuffed with interstitial Ba (blue) and infinite linear chains (green) along *b* axis formed by Zn atoms in BaAu<sub>3</sub>Zn<sub>2</sub> structure.

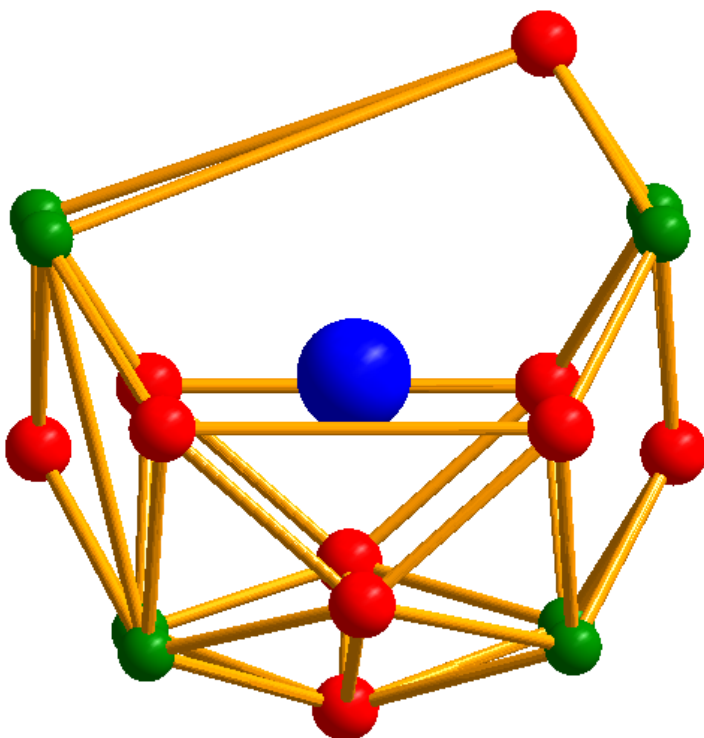


**Figure 3.** The environment of interstitial Ba atom, formed by Au and Zn atoms result in a cage -like structure.

### 3.2. Bonding

Today, bonding characteristics of extended solids remain one of the central and challenging topics in solid-state chemistry despite seeing rapid growth of the discovery of new intermetallic and metal-rich compounds during the past decades. For bonding analysis, the energy contributions of all filled electronic states of neighboring atom

pairs were calculated by the crystal orbital Hamilton population (COHP) method [24, 25]. The total and partial densities-of-states (DOS) and the crystal orbital Hamilton populations (-COHP) are given in Figure 4.

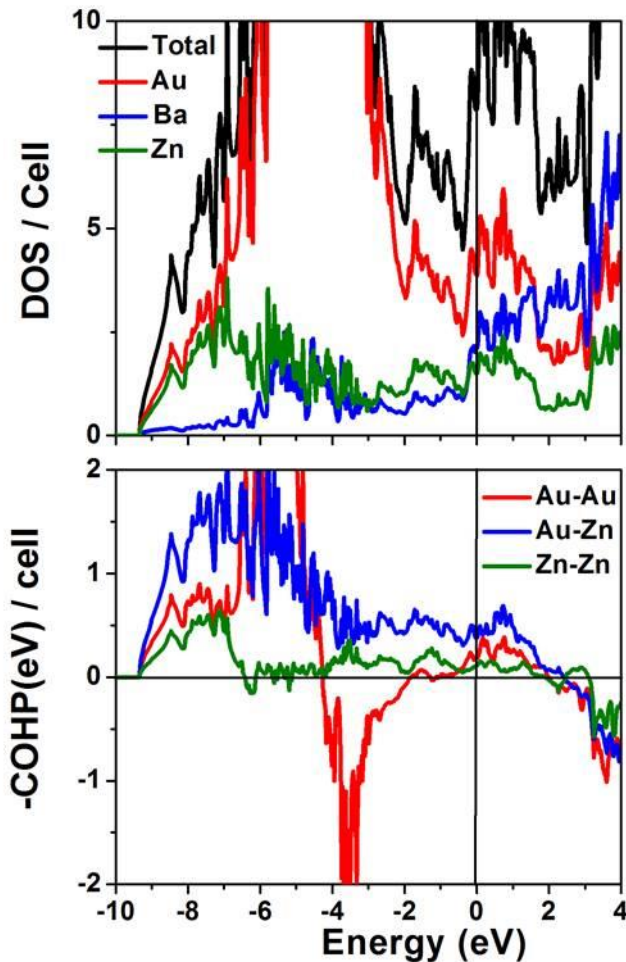


**Figure 4.** The density-of-states (DOS) and crystal orbital Hamilton population (COHP) data for BaAu<sub>3</sub>Zn<sub>2</sub>. Densities-of-states (DOS) for different atom types (top). COHP curves (bottom): Au–Au (red), Au–Zn (blue), Zn–Zn (green).

The calculation shows a typical polar intermetallic behavior for BaAu<sub>3</sub>Zn<sub>2</sub>. The presence of continuous bands at the Fermi energy ( $E_F$ ) indicates that present phase has metallic characters. The orbital DOS shows the dominance of split Au 5d states in its bonding region with some extending above  $E_F$ . Integrated COHP data (-ICOHP) for specific bonds and their contributions are listed in Table 3.

**Table 3.** Bond length and -ICOHP values for BaAu<sub>3</sub>Zn<sub>2</sub>.

Bond	length (Å)	-ICOHP (eV/per bond)	n/cell	-ICOHP (eV/cell)	%
Au-Au	2.771-3.054	1.00	22	22.00	20.0
Au-Zn	2.596-2.812	1.35	45	60.75	55.0
Zn-Zn	2.737-2.756	0.84	8	6.72	6.1
Ba-Au	3.381-3.501	0.43	36	15.48	14.0
Ba-Zn	3.792-3.860	0.17	32	5.44	4

As expected from bond distances, Au-Zn, Au-Au and Zn-Zn have large -ICOHP values *i.e.* 1.35, 1.00 and 0.84eV/bond, whereas Ba-Au and Ba-Zn have small values (0.43 and 0.17 eV/bond). Au-Zn has the largest -

ICOHP value, 1.35 eV/bond and its total contribution to the entire unit is 55%. This situation is similar to those in  $\text{Ba}_2\text{Au}_6(\text{Au},\text{Zn})_3$  [5],  $\text{Sr}_2\text{Au}_6(\text{Au},\text{Zn})_3$  [6] and  $\text{CaAu}_4\text{Zn}_2$  systems which means that Au-Zn interaction is again dominant and its contribution is essential to form the 3D  $\text{Au}_3\text{Zn}_2$  network. The Au-Au (bond distance 2.771-3.054 Å, 1.0 eV/bond) in the present structure is comparable to those in 2-6-3 structures (2.6-3.0 Å, ~1.2 eV/bond) and  $\text{CaAu}_4\text{Zn}_2$  system (2.8 Å, ~1.3 eV/bond). The Zn-Zn (bond distance ~ 2.74 Å, 0.84 eV/bond) bonding in the linear chain contributes nearly 6% to the unit which is comparable to the Zn-Zn contribution observed for the Zn-linear chain in  $\text{CaAu}_4\text{Zn}_2$  system (bond distance 2.678 Å, 1.02 eV/bond). The Au-Au, Zn-Zn and Au-Zn bonds show either bonding or nonbonding character, indicating an optimized structure for  $\text{BaAu}_3\text{Zn}_2$ . Ba-Au and Ba-Zn interactions contribute less (total ~19%) to the stability of  $\text{BaAu}_3\text{Zn}_2$  structure. The above outcome strongly suggests significant multi-centered bonding that leads to their structural and phase stability.

#### 4. Conclusion

The bonding characteristics of valence electron-poor polar intermetallics, features that are significant for cohesion and chemistry, is a debatable topic in solid-state chemistry. In continuation, we have discovered the intermetallic compound  $\text{BaAu}_3\text{Zn}_2$ . The structure has mainly three components: hexagonal-diamond-like gold host lattice, interstitial Ba atoms and infinite linear chains along *b* axis formed by only Zn atoms. Although  $\text{BaAu}_3\text{Zn}_2$  and  $\text{SrZn}_5$  have similar Pearson symbol and same set of Wyckoff positions but they exhibit different bonding patterns, which render them as different structural types.  $\text{BaAu}_3\text{Zn}_2$  structure contains the hexagonal-diamond-like gold host lattice which is comparable to the unprecedented hexagonal-diamond-like gold host lattice, observed in the series  $\text{A}_2\text{Au}_6(\text{Au},\text{T})_3$ , (A= Ba, Sr and T = Al, Cd, Ga, In, Sn, Zn). Fermi energy ( $E_F$ ) indicates that present phase has metallic characters and bonding analyses indicate a typical polar intermetallics behavior for  $\text{BaAu}_3\text{Zn}_2$ .

#### Acknowledgements

This research is supported by the U.S. National Science Foundation, Solid State Chemistry, via Grant DMR-0853732. All the work is performed in the facilities of the Ames Laboratory, U.S. Department of Energy (DOE).

#### References

- [1] J. D. Corbett, *Inorg. Chem.* **2010**, 49, 13.
- [2] Q. Lin, J. D. Corbett, In *Struct. Bond.*; Wu, X.-T., Ed.; Springer Berlin / Heidelberg, **2009**, 133, 1-39.
- [3] G. J. Miller, *Eur. J. Inorg. Chem.* **1998**, 523-536.
- [4] P. Pyykkö, *Angew. Chem. Int. Ed.* **2002**, 41, 3573.
- [5] Q. Lin, T. Mishra, J. D. Corbett, *J. Am. Chem. Soc.* **2013**, 135, 11023.
- [6] T. Mishra, Q. Lin, J. D. Corbett, *Inorg. Chem.* **2013**.
- [7] V. Smetana, G. J. Miller, J. D. Corbett, *Inorg. Chem.* **2013**, 52, 12502.
- [8] B. Gerke, O. Niehaus, R. D. Hoffmann, R. Z. Pöttgen, *Anorg. Allg. Chem.* **2013**, 639, 2575.
- [9] T. Mishra, Q. Lin, J. D. Corbett, *J. Solid State Chem.* **2014**, 218, 103-108.
- [10] U. Mizutani, Hume-Rothery Rule for Structurally Complex Alloy Phases; CRC Press:London, **2011**.
- [11] W. Kraus, G. Nolze, In *Powder Cell for Windows*. [http://www.bam.de/de/service/publikationen/powder\\_cell.htm](http://www.bam.de/de/service/publikationen/powder_cell.htm).
- [12] T. J. B. Holland, S. A. T. Redfer, *Mineral. Mag.* **1997**, 61, 65.
- [13] V. Petricek, M. Dusek, L. Palatinus, *Jana2006. The crystallographic computing system* Institute of Physics, Praha, Czech Republic **2006**.
- [14] *SHELXTL 6.10 ed.*, Bruker Analytical X-ray Systems, Inc., Madison, WI. **2000**.
- [15] H. L. Shriver, *The LMTO Method; The LMTO Method*, Springer-Verlag, Berlin, Germany, **1984**.
- [16] Raub, C. J.; Hamilton, D. C. *J. Less-Comm. Met.* **1964**, 6, 486.
- [17] R. Tank, O. Jepsen, A. Burkhardt, O. K. Andersen, *TB-LMTO-ASA Program, Vers. 4.7*, TB-LMTO-ASA Program, Vers. 4.7, Max-Planck-Institut für Festkörperforschung, Stuttgart, Germany, **1994**.

- [18] L. Pauling, *The Nature of the Chemical Bond*; 3rd ed.; Cornell University Press: Ithaca, NY, **1960**.
- [19] Q. Lin, J. D. Corbett, *Inorg. Chem.* **2010**, *49*, 4570.
- [20] A. P. Tsai, J. Q. Guo, E. Abe, H. Takakura, T. J. Sato, *Nature* **2000**, *408*, 537.
- [21] B. Li, J. D. Corbett, *J. Am. Chem. Soc.* **2006**, *128*, 12392.
- [22] Q. Lin, J. D. Corbett, *Inorg. Chem.* **2008**, *47*, 7651.
- [23] Q. Lin, J. D. Corbett, *Inorg. Chem.* **2010**, *49*, 10436.
- [24] R. Dronskowski, P. E. Bloechl, *J. Phys. Chem.* **1993**, *97*, 8617.
- [25] J. Ren, W. Liang, M.-H. Whangbo, *CAESAR for Windows*; Prime-Color Software, Inc., North Carolina State University: Raleigh, NC, 1998.